Dynamics of the Simplest Chlorine Atom Reaction: An Experimental and Theoretical Study

M. Alagia, N. Balucani, L. Cartechini, P. Casavecchia,* E. H. van Kleef, G. G. Volpi, F. J. Aoiz,* L. Bañares, D. W. Schwenke, T. C. Allison, S. L. Mielke, D. G. Truhlar*

Angular distributions and time-of-flight spectra for the reaction Cl + H_2 → HCl + H obtained from a high-resolution, crossed-molecular beam experiment were compared to differential cross sections calculated by both converged quantum mechanical scattering and quasi-classical trajectory methods. Good agreement was found between the experimental results and each theoretical prediction. The results demonstrate that excellent agreement can be obtained between state-of-the-art simulations and experiments for the detailed dynamical properties of this prototype chlorine atom reaction.

The fundamental goal of chemical reaction dynamics is to learn about the forces that control chemical reactivity, that is, for each chemical reaction to learn about the nature of the potential energy surface (PES) that governs the nuclear motions. Our goal is to model the PES well enough to predict the detailed dynamics of reactions. The physical observables most sensitive to the nature of the PES are reaction cross sections, especially differential cross sections (*1*, *2*). If converged quantum mechanical (QM) scattering calculations on an assumed PES can be performed, a comparison of calculated and experimental cross sections provides a sensitive test of our ability to predict detailed dynamical attributes of reactions. To date, this kind of test has only been applied to the D + H_2 (*3*), H + D_2 (*4*), and F + H_2 reactions (*5*). In this report we extend this fundamental comparison to a third chemical reaction:

$$Cl + H_2 \rightarrow HCl + H \qquad (1)$$

for which the heat of reaction is ΔH°_0 = 1.03 kcal/mol. The interest of chemical kineticists in this system dates back to the 19th century when the reaction was studied by Draper (1843), Bunsen and Roscoe (1857), and van't Hoff. Later work on this reaction included pioneering studies (*6*) in connection with the mechanism of the H_2-Cl_2 chain reaction, for which reaction 1 is the rate-determining step. Reaction 1 has played a central role in fundamental chemical kinetics and has served as a critical test case for bimolecular reaction rate theory, especially transition-state and kinetic isotope effect (KIE) theories (*7*). This reaction is also a prototype for a host of Cl reactions that are important in atmospheric chemistry and photochemical air pollution.

Experimental work on the rate constants of reaction 1 and its H isotopic variants was recently summarized (*8*). However, cross sections have not been determined to date. The HCl product from reaction 1 can only be formed in the ground vibrational level for low relative translational energies E_{rel} (Fig. 1A); this limitation rules out the application of infrared chemiluminescence (*9*) to detect products. The products can be detected with a mass spectrometer in a crossed molecular beam (CMB) arrangement, but this procedure is very challenging because of a high barrier, a near mass conflict of the product with the second most abundant Cl isotope, and unfavorable kinematics.

Early work on the ClH_2 PES, reviewed elsewhere (*10*), was quantitatively and sometimes qualitatively unreliable. In 1973, Stern *et al.* (*11*) created three semiempirical PESs (*7*) that yielded good accuracy for KIEs of the Cl + H_2 reaction but were inaccurate for H-Cl-H geometries. An improved global PES was proposed by Baer and Last (*12*); unfortunately, it predicted rate constants and KIEs less accurately (*13*) than the earlier PESs. A more successful surface, called GQQ, based in part on electronic structure calculations with scaled electron correlation for H-Cl-H type geometries, was published in 1989 (*14*). Recently, a new PES (Fig. 1B), called G3, was created. It has, with respect to GQQ, a slightly larger (by 0.18 kcal/mol) barrier height and an improved Cl-H-H bend potential obtained by ab initio methods (*15*). This PES also yields agreement with thermal rate constants and KIEs for the Cl + H_2 reaction (*16*), so it is useful to test whether it can be used to accurately simulate the detailed dynamics of this reaction.

Early theoretical work on the dynamics of reaction 1 was based on conventional transition-state theory, trajectory calculations, reduced-dimensionality QM studies, variational transition-state theory with multidimensional tunneling, and approximate QM scattering calculations (*17*). In 1991, converged QM scattering calculations for the Cl + H_2 reaction on the GQQ surface were reported (*18*).

In this report, we present the results of a CMB investigation of reaction 1. We obtained differential cross sections (DCSs) for E_{rel} = 5.85 kcal/mol for

$$Cl(^2P_{3/2,\,1/2}) + n - H_2(v = 0, j = 0,1,2,3) \rightarrow$$
$$HCl(v' = 0, \text{all } j') + H \qquad (2)$$

where v (v') and j (j') are reactant (product) vibrational and rotational quantum numbers, by measuring angular and velocity distributions of the HCl(v' = 0) product.

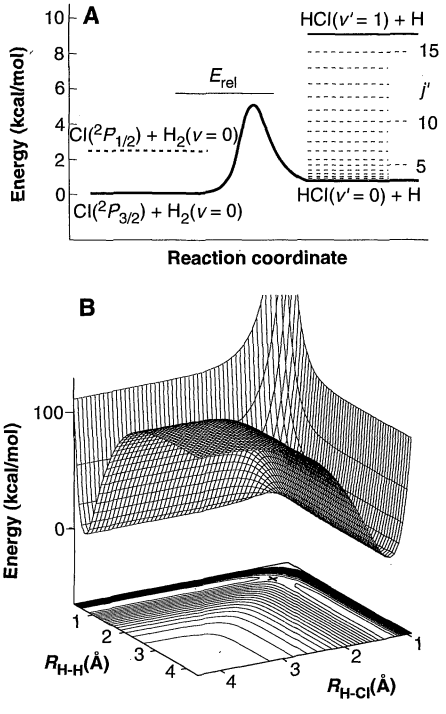

Fig. 1. (**A**) Energy level diagram for the Cl + H_2 reaction with the spin-orbit levels of the reactants and the rovibrational levels of the products indicated. The effective potential energy barrier of the G3 surface, including zero-point energy for reactant, product, and modes transverse to reaction coordinate, is shown as a solid curve. The relative translational energy of the experiment, E_{rel}, is indicated with a line. (**B**) Contour map and three-dimensional perspective of the G3 PES for the colinear Cl-H-H arrangement. The saddle point, of height 7.88 kcal/mol, is denoted by an ×. R is the distance between the specified atoms.

M. Alagia, N. Balucani, L. Cartechini, P. Casavecchia, E. H. van Kleef, G. G. Volpi, Dipartimento di Chimica, Universita di Perugia, 06100 Perugia, Italy.
F. J. Aoiz and L. Bañares, Departamento de Química Física, Facultad de Química, Universidad Complutense, 28040 Madrid, Spain.
D. W. Schwenke, NASA Ames Research Center, Mail Stop 230-3, Moffett Field, CA 94035, USA.
T. C. Allison, S. L. Mielke, D. G. Truhlar, Department of Chemistry, Chemical Physics Program, and Supercomputer Institute, University of Minnesota, Minneapolis, MN 55455, USA.
*To whom correspondence should be addressed.

We also carried out scattering calculations of state-to-state ($v, j \rightarrow v', j'$) DCSs based on accurate QM methods as well as the quasiclassical trajectory (QCT) method, in both cases using the G3 PES. The theoretical DCSs, after transformation into the laboratory frame and experimental averaging, were compared directly with the laboratory data, thus providing a direct test of the ground–electronic state PES of Cl + H_2.

The CMB apparatus has been described in detail elsewhere (*19*). Two well-collimated supersonic beams of the reagents are crossed at 90° in a large scattering chamber maintained in the 10^{-7}-mbar range. An electron impact quadrupole mass spectrometer, contained in an ultrahigh-vacuum (10^{-11} mbar) chamber, serves as the detector of the reaction products. The product angular distribution is measured by rotating the detector in the collision plane around an axis that passes through the collision center. The velocities of the products are derived from pseudorandom time-of-flight (TOF) measurements (*20*).

A supersonic beam of Cl atoms was generated from a high-pressure, high-power radio-frequency discharge beam source (*19*), starting from dilute mixtures of Cl_2 in He with some O_2 added to moderate the plasma temperature and stabilize the discharge. This procedure leads to 98% dissociation of molecular Cl_2. The beam had an angular divergence of 1.5°, a peak velocity of 2650 m/s, and a velocity spread of 20%. The $Cl(^2P_{3/2,1/2})$ spin-orbit distribution was characterized by Stern-Gerlach magnetic analysis, as done in the Perugia laboratory for effusive beams of Cl (*21*). About 90% of the Cl atoms were found to be in the ground $^2P_{3/2}$ electronic state, and 10% were in the excited $^2P_{1/2}$ state. We could vary the concentration of $Cl(^2P_{1/2})$ by changing the seeding gas.

We generated a supersonic beam of H_2 by allowing pure H_2 to expand at high stagnation pressure through a stainless steel nozzle kept at about 800 K to increase the beam translational energy. The beam had an angular divergence of 2.9°, a peak velocity of 4401 m/s, and a velocity spread of 15%. We estimated that the rotational temperature of the normal-$H_2(j)$ reagent molecules in the beam under our expansion conditions was about 300 K by extrapolating the consistent experimental determination of Pollard *et al.* (*22*). The corresponding relative rotational populations were 0.13, 0.66, 0.12, and 0.09 for j = 0, 1, 2, and 3, respectively.

The laboratory angular distribution of the HCl product (detected at a mass/charge ratio m/e = 38) from the $Cl(^2P_{3/2,1/2}) + H_2$ reaction was determined at E_{rel} = 5.85 kcal/mol (Fig. 2). Product velocity distributions were recorded at four different angles (Fig. 3). In a series of experiments carried out on the Cl + D_2 reaction at several collision energies starting at E_{rel} = 4.75 kcal/mol and using Cl beams containing 10 or 25% of spin-orbit excited state, we found that product angular and velocity distributions could be fitted without invoking a contribution from $Cl(^2P_{1/2})$, which has an additional energy of 2.5 kcal/mol (Fig. 1A). Thus, the contribution of $Cl(^2P_{1/2})$ is negligible, and the HCl angular distribution shown in Fig. 2 corresponds to the $Cl(^2P_{3/2}) + H_2$ reaction.

The product is almost completely confined to the right of the center-of-mass (CM) angle in the laboratory frame, that is, in the backward direction with respect to the Cl beam, and it is sharply peaked at an angle nearly tangent to the maximum Newton circle, within which the product can be scattered on the basis of energy and linear momentum conservation (Fig. 2). These features suggest that the mechanism of the reaction is direct and is of the rebound type (*2*) and that a very large fraction of the available energy is disposed into relative translational motion of the products.

We carried out full-dimensional QM calculations of state-to-state DCSs for reaction 2 with j = 0, 1, and 2, using methods described in (*23*), at a total energy of 12.19 kcal/mol, which corresponds to an initial relative translational energy of 6.0, 5.66, and 4.98 kcal/mol for H_2 in j = 0, 1, and 2, respectively. Calculations of the same quantities were also performed by the QCT method, as described in (*24*), at the experimental E_{rel} = 5.85 kcal/mol for all the relevant rotational levels (j = 0, 1, 2, and 3) of H_2. The QCT method is based on trajectories that are fully classical except for the selection of initial conditions and the interpretation of the final states. These calculations were performed to test the validity of classical simulations for predicting product state distributions for a simple three-atom reaction in which two of the atoms are H atoms, which are expected to exhibit the largest quantum effects because of their small mass.

Absolute initial state–selected DCSs for formation of HCl(v' = 0), summed over all final rotational levels j' and the absolute HCl(v' = 0) integral cross sections for specific j' were obtained from the QCT and QM calculations (Fig. 4). There is reasonably good agreement between the QM and QCT results; in particular, the QM and QCT rotational distributions peak at the same j' values. However, at E_{rel} = 6.0 kcal/mol the QM DCS for Cl + $H_2(j = 0) \rightarrow$ HCl, summed over all final j', is slightly larger (by 8% at a CM angle θ = 180°) than that obtained from QCT calculations.

We carried out a detailed comparison of the experimental results with the theoretical predictions by averaging the QCT and QM cross sections over the experimental conditions. The laboratory angular and

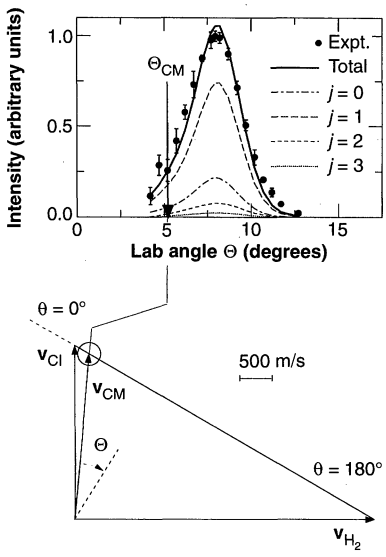

Fig. 2. The HCl(v' = 0) product laboratory angular distribution from the Cl + $H_2(j$ = 0, 1, 2, 3) reaction at relative translational energy E_{rel} = 5.85 kcal/mol and the corresponding canonical velocity vector ("Newton") diagram; $\mathbf{v}_{H_2}$ and $\mathbf{v}_{Cl}$ are the laboratory beam velocity vectors; $\mathbf{v}_{CM}$ is the CM velocity vector; θ and Θ are CM and laboratory scattering angles, respectively; and Θ_{CM} is the angle between $\mathbf{v}_{Cl}$ and $\mathbf{v}_{CM}$. The circle in the Newton diagram indicates the maximum speed that the HCl product can attain, if all the available energy is channeled into translation, that is, the speed of HCl(v' = 0, j' = 0). The solid line represents the angular distribution obtained from QCT calculations on the G3 PES. The separate contributions from rotational levels of H_2 are also indicated.

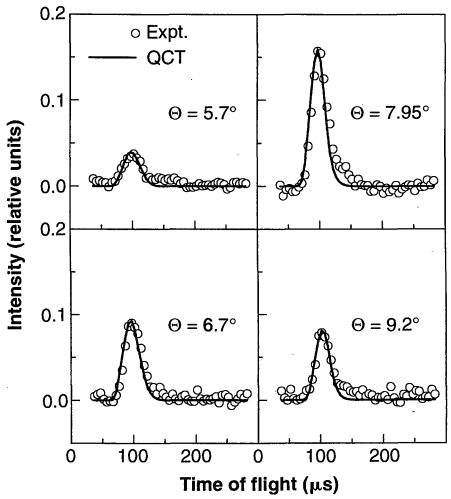

Fig. 3. The HCl(v' = 0) product time-of-flight distributions at selected laboratory angles Θ from the Cl + $H_2(j$ = 0, 1, 2, 3) reaction at E_{rel} = 5.85 kcal/mol. Solid lines are as in Fig. 2.

TOF distributions of Figs. 2 and 3 contain information on the rotational state distribution of HCl($v' = 0$), which should be sensitive to the interatomic torques during the collision and hence should provide a critical test of the PES, especially the effective barrier height as a function of bond angle. The rotational distributions for each initial j level of H_2 (Fig. 4, C and D) were found in both QCT and QM calculations to not vary greatly with scattering angle. They were converted into translational energy distributions, $P_j(E)$, for each initial j of H_2 and treated as continuous functions. The CM total DCS for HCl($v' = 0$) was obtained according to

$$I_{CM}(\theta, E) = \sum_{j=0,1,2,3} w_j T_j(\theta) P_j(E) \quad (3)$$

where w_j are the relative weights of the H_2 rotational levels in the beam, the $T_j(\theta)$ functions are the calculated CM DCSs for each initial j of H_2 summed over all j' shown in Fig. 4, A and B, and the $P_j(E)$ functions are obtained from the rotational distributions of Fig. 4, C and D, as discussed above. The DCS for each initial j was transformed into the laboratory frame and averaged over the finite resolution of experimental conditions, taking into account the strong energy dependence of the reactive integral cross section, as calculated by QCT.

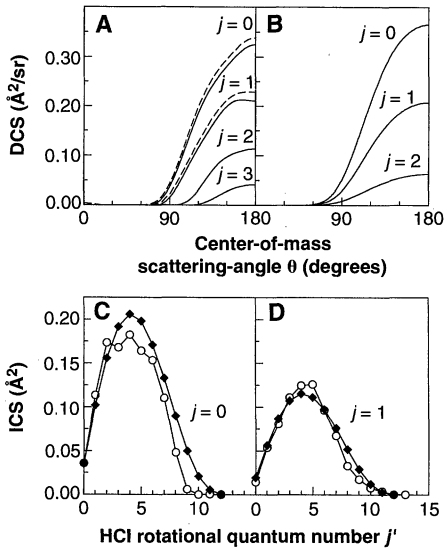

Fig. 4. (**A**) Angular dependence of the CM differential cross section (DCS) for the HCl($v' = 0$) product of the Cl + H_2($v = 0, j$) reaction obtained from QCT calculations at a relative translational energy of 5.85 kcal/mol for all initial j values of H_2 (solid lines) and of 6.0 kcal/mol for $j = 0$ and $j = 1$ (dashed lines). (**B**) The same from QM calculations at a translational energy E_{rel} = 6.0 kcal/mol for $H_2(j = 0)$, E_{rel} = 5.66 kcal/mol for $H_2(j = 1)$, and E_{rel} = 4.98 kcal/mol for $H_2(j = 2)$. The same G3 PES was used for both QM and QCT calculations. (**C** and **D**): Integral state-to-state cross sections (ICSs) for selected rotational levels j' of the HCl($v' = 0$) product from $H_2(j = 0)$ (C) and $H_2(j = 1)$ (D): (○) QCT calculations at E_{rel} = 5.85 kcal/mol; (◆) QM calculations at E_{rel} = 6.0 kcal/mol for $H_2(j = 0)$ and E_{rel} = 5.66 kcal/mol for $H_2(j = 1)$.

We found quite good agreement between the QCT results and the experimental data (see Figs. 2 and 3). A similar comparison was carried out between the QM results and experiment. In this case the DCS calculated for $H_2(j = 1)$ at E_{rel} = 5.66 kcal/mol was also used for $H_2(j = 0, 2,$ and $3)$. This approximation should be warranted, at least within the sensitivity of the experimental data, because (i) QCT calculations indicate that the DCS at E_{rel} = 5.85 kcal/mol differs very little from that at E_{rel} = 6.0 kcal/mol (see Fig. 4A), (ii) the angular dependence of the DCS is nearly independent of the initial j state of H_2 (see Fig. 4, A and B), and (iii) $H_2(j = 0)$ and $H_2(j = 1)$ give the dominant contribution to the measured TOF and angular distributions (Fig. 2). The laboratory distributions calculated from the QM results are practically indistinguishable, on the scale of Figs. 2 and 3, from those obtained from the QCT results. The QCT calculations are in remarkably good overall agreement with the exact QM results. Similar agreement has also been observed for the H + D_2 (*3*, *4*, *25*), D + H_2 (*26*), and F + H_2 (*27*) reactions.

The sharp peaking of the laboratory angular distribution in the backward direction is well reproduced by theory (see Fig. 2), which predicts that the CM DCS is strongly peaked at $\theta = 180°$ (Fig. 4, A and B). Both QM and QCT calculations indicate that 80% of the total available energy is deposited into translation. The theoretical calculations predict very little variation of the product rotational excitation with the scattering angle, again in agreement with experiment. Indeed, the TOF data are well reproduced (Fig. 3), if we assume the same rotational distribution within $\theta = 90°$ and $\theta = 180°$ (the range of the CM DCS), as expressed by Eq. 2. The good agreement between theory and experiment shows that simulations based on the G3 PES provide a quantitatively accurate model of the detailed dynamics of the simplest Cl reaction.

REFERENCES AND NOTES

1. R. D. Levine and R. B. Bernstein, *Molecular Reaction Dynamics and Chemical Reactivity* (Oxford Univ. Press, New York, 1987).
2. D. R. Herschbach, *Adv. Chem. Phys.* **10**, 319 (1966).
3. W. H. Miller, *Annu. Rev. Phys. Chem.* **41**, 245 (1990); R. E. Continetti, J. Z. H. Zhang, W. H. Miller, *J. Chem. Phys.* **93**, 5356 (1990); R. E. Continetti, B. A. Balko, Y. T. Lee, *ibid.*, p. 5719; M. Zhao, D. G. Truhlar, D. W. Schwenke, *J. Phys. Chem.* **94**, 7074 (1990); D. A. V. Kliner, D. E. Adelman, R. N. Zare, *J. Chem. Phys.* **95**, 1648 (1991); S. L. Mielke, R. S. Friedman, D. G. Truhlar, D. W. Schwenke, *Chem. Phys. Lett.* **188**, 359 (1992); A. Kuppermann and Y.-S. M. Wu, *ibid.* **205**, 599 (1993).
4. T. N. Kitsopoulos, M. A. Buntine, D. P. Baldwin, R. N. Zare, D. W. Chandler, *Science* **260**, 1605 (1993); S. L. Mielke, D. G. Truhlar, D. W. Schwenke, *J. Phys. Chem.* **98**, 1053 (1994); F. J. Aoiz *et al.*, *J. Chem. Phys.* **101**, 5781 (1994); L. Schnieder *et al.*, *Science* **269**, 207 (1995).
5. Y. T. Lee, *Science* **236**, 793 (1987); D. M. Neumark, A. M. Wodtke, G. N. Robinson, C. C. Hayden, Y. T. Lee, *J. Chem. Phys.* **82**, 3045 (1985); S. L. Mielke, G. C. Lynch, D. G. Truhlar, D. W. Schwenke, *Chem. Phys. Lett.* **213**, 10 (1993); D. E. Manolopoulos *et al.*, *Science* **262**, 1852 (1993); M. Baer *et al.*, *J. Chem. Phys.* **104**, 2743 (1995); J. F. Castillo, D. E. Manolopoulos, K. Stark, H.-J. Werner, *ibid.*, p. 6531.
6. D. L. Chapman and L. K. Underhill, *J. Chem. Soc.* **103**, 496 (1913); M. Bodenstein and W. Dux, *Z. Phys. Chem. (Leipzig)* **85**, 297 (1913); W. Nernst, *Z. Elektrochem.* **24**, 335 (1918).
7. H. Eyring and M. Polanyi, *Z. Phys. Chem. (Leipzig) Abt. B* **12**, 279 (1931); J. O. Hirschfelder, H. Eyring, B. Topley, *J. Chem. Phys.* **4**, 170 (1936); A. Wheeler, B. Topley, H. Eyring, *ibid.*, p. 178; S. Sato, *ibid.* **23**, 2465 (1955); K. J. Laidler, *Chemical Kinetics* (Harper & Row, New York, ed. 3, 1987), pp. 14, 288–298.
8. S. S. Kumaran, K. P. Lim, J. V. Michael, *J. Chem. Phys.* **101**, 9487 (1994).
9. J. C. Polanyi, *Science* **236**, 680 (1987).
10. C. A. Parr and D. G. Truhlar, *J. Phys. Chem.* **75**, 1844 (1971).
11. M. J. Stern, A. Persky, F. S. Klein, *J. Chem. Phys.* **58**, 5697 (1973).
12. M. Baer and I. Last, in *Potential Energy Surfaces and Dynamics Calculations*, D. G. Truhlar, Ed. (Plenum, New York, 1981), p. 519.
13. S. C. Tucker, D. G. Truhlar, B. C. Garrett, A. D. Isaacson, *J. Chem. Phys.* **82**, 4102 (1985).
14. D. W. Schwenke *et al.*, *ibid.* **90**, 3110 (1989).
15. T. C. Allison, G. C. Lynch, D. G. Truhlar, M. S. Gordon, *J. Phys. Chem.*, in press.
16. S. L. Mielke, T. C. Allison, D. G. Truhlar, D. W. Schwenke, *ibid.*, in press.
17. M. Salomon, *Int. J. Chem. Kinet.* **2**, 175 (1970); D. L. Thompson, H. H. Suzukava Jr., L. M. Raff, *J. Chem. Phys.* **62**, 4727 (1975); A. Persky, *ibid.* **66**, 2932 (1977); *ibid.* **68**, 2411 (1978); *ibid.* **70**, 3910 (1979); A. Persky and M. Broida, *ibid.* **84**, 2653 (1986); A. Persky and M. Baer, *ibid.* **60**, 133 (1974); B. C. Garrett, D. G. Truhlar, A. W. Magnuson, *ibid.* **76**, 2321 (1982); D. C. Clary, *Chem. Phys. Lett.* **80**, 271 (1981); V. J. Barclay, B. A. Collings, J. C. Polanyi, J. H. Wang, *J. Phys. Chem.* **95**, 2921 (1991); S. Takada, K. Tsuda, A. Ohsaki, H. Nakamura, in *Advances in Molecular Vibrations and Collision Dynamics*, J. M. Bowman, Ed. (JAI Press, Greenwich, CT, 1994), vol. 2A, p. 245.
18. J. M. Launay and S. B. Padkjaer, *Chem. Phys. Lett.* **181**, 95 (1991); S. E. Branchett, S. B. Padkjaer, J. M. Launay, *ibid.* **208**, 523 (1993).
19. M. Alagia, N. Balucani, P. Casavecchia, D. Stranges, G. G. Volpi, *J. Chem. Soc. Faraday Trans.* **91**, 575 (1995); *J. Chem. Phys.* **98**, 2459 (1993); *ibid.*, p. 8341.
20. K. Sköld, *Nucl. Instrum. Methods* **63**, 114 (1968).
21. V. Aquilanti, R. Candori, D. Cappelletti, V. Lorent, F. Pirani, *Chem. Phys. Lett.* **192**, 145 (1992); *J. Chem. Soc. Faraday Trans.* **89**, 1467 (1993).
22. J. E. Pollard, D. J. Trevor, Y. T. Lee, D. A. Shirley, *J. Chem. Phys.* **77**, 4818 (1982).
23. G. J. Tawa, S. L. Mielke, D. G. Truhlar, D. W. Schwenke, *ibid.* **100**, 5751 (1994).
24. F. J. Aoiz and L. Bañares, *Chem. Phys. Lett.* **247**, 232 (1995).
25. M. Zhao, D. G. Truhlar, N. C. Blais, D. W. Schwenke, D. J. Kouri, *J. Phys. Chem.* **94**, 6696 (1990).
26. F. J. Aoiz, V. J. Herrero, V. Sáez-Rábanos, *J. Chem. Phys.* **97**, 7423 (1992); S. L. Mielke, G. C. Lynch, D. G. Truhlar, D. W. Schwenke, *J. Phys. Chem.* **98**, 8000 (1994); F. J. Aoiz, L. Bañares, T. Diez-Rojo, V. J. Herrero, V. Sáez-Rábanos, *ibid.* **100**, 4071 (1996).
27. F. J. Aoiz, L. Bañares, V. J. Herrero, V. Sáez-Rábanos, *Chem. Phys. Lett.* **218**, 422 (1994); ———, K. Stark, H.-J. Werner, *ibid.* **223**, 215 (1994); *J. Phys. Chem.* **98**, 10665 (1994).

28. This work was supported by the Italian "Consiglio

Nazionale delle Ricerche–Progetto Finalizzato Chimica Fine" and "Ministero Università e Ricerca Scientifica"; grants from the European Economic community, the Italian Ente per le Nuove Tecnologie, l'Energia e l'Ambiente, NATO (CRG 920549), and the Air Force Office of Scientific Research (grant F617-08-94-C-0013) through the European Office of Aerospace Research and Development (grant SPC-94-4042); and the Dirección General de Investigación Científica y Tecnológica of Spain under grant PB95-0918-C02. This work was supported in part by the NSF under grant CHE 94-23927.

29 May 1996; accepted 24 July 1996

The Effect of Alumina on Phase Transformations at the 660-Kilometer Discontinuity from Fe-Mg Partitioning Experiments

B. J. Wood and D. C. Rubie

Experimental data on the partitioning of Fe and Mg between coexisting silicate perovskite, magnesiowüstite, and γ-$(Mg,Fe)_2SiO_4$ demonstrate that Fe substitution in perovskite is strongly coupled to Al_2O_3 concentration. In Al_2O_3-free compositions, perovskite has a low Fe/(Fe+Mg) ratio: for a bulk Fe/(Fe+Mg) of 0.11, perovskite has a value close to 0.04, whereas magnesiowüstite has a ratio near 0.17. In peridotitic mantle, however, where the perovskite should contain 4 to 5 weight percent Al_2O_3, it has essentially the same Fe/(Fe+Mg) ratio as coexisting magnesiowüstite. Under lower mantle conditions, therefore, perovskite and magnesiowüstite should, in peridotite, each have an Fe/(Fe+Mg) ratio close to 0.11.

The seismic discontinuity at 660-km depth is a global feature, dividing Earth's lower mantle from the overlying transition zone and upper mantle. It corresponds to 6 to 10% increases in seismic wave velocity and density with increasing depth (*1*). Recent experiments (*2–4*) have demonstrated that the 660-km discontinuity corresponds in pressure (23.5 GPa) and temperature (approximately 1600°C) to the conditions of the decomposition of γ-$(Mg,Fe)_2SiO_4$ spinel (SP), the major constituent of peridotite at this depth (*3*), into $(Mg,Fe)SiO_3$ perovskite (PV) and (Mg,Fe)O magnesiowüstite (MW)

$$\underset{\text{SP}}{(Mg,Fe)_2SiO_4} = \underset{\text{PV}}{(Mg,Fe)SiO_3} + \underset{\text{MW}}{(Mg,Fe)O} \quad (1)$$

The documentation of such conditions means that a qualitative interpretation of the 660-km discontinuity can be provided by the occurrence of reaction 1 in an approximately peridotitic mantle (*3*). Better constraints on average mantle composition are, in principle, provided by the sharpness and magnitudes of density and seismic velocity changes at the 660-km discontinuity and from velocity and density gradients in the lower mantle (*5*). However, in order to compare seismically determined density and velocity structure with laboratory-measured elastic properties and densities of minerals, it is necessary to know how the chemical components of the mantle distribute themselves between the different minerals present. Currently, the partitioning of FeO, MgO, and other major components such as Al_2O_3 between perovskite and magnesiowüstite is poorly constrained for peridotitic and other natural compositions. Therefore, partitioning behavior must be assumed, yielding uncertain estimates of bulk rock properties. The partitioning assumptions are important because density and elastic properties depend substantially on compositional parameters such as Fe#, the molar ratio Fe/(Fe+Mg). Here we determine the partitioning of Fe and Mg between spinel, perovskite, and magnesiowüstite in bulk compositions that reflect natural abundances of minor components such as Al_2O_3 in order to obtain better estimates of mineral compositions under lower mantle conditions. The results are also applied to an understanding of the reactions at depths between 660 and 750 km.

All experiments were performed on the multianvil apparatus at the Bayerisches Geoinstitut, and analyses were made with the JEOL 8600 microprobe at the University of Bristol (*6*). Our data (Table 1) on the partitioning of Fe and Mg between spinel and magnesiowüstite in compositions doped with about 1% each of Al_2O_3, MnO, Cr_2O_3, and NiO are consistent with previous results (*4*, *7*, *8*) in both peridotitic bulk compositions and in the simple system $MgO\text{-}FeO\text{-}SiO_2$. The magnesiowüstite is always substantially richer in Fe than is coexisting spinel. For typical peridotite with an Fe# in spinel of 0.11, the coexisting magnesiowüstite would have an Fe# of 0.166. On the basis of a comparison with previous results, we find that doping with Al_2O_3, MnO, Cr_2O_3, and NiO does not significantly affect the Fe-Mg partitioning between spinel and magnesiowüstite. Partitioning data for Fe and Mg between perovskite and magnesiowüstite in Al_2O_3-free compositions (*8–11*) indicate that perovskite in equilibrium with magnesiowüstite contains very little Fe. A perovskite Fe# of about 0.04 would be appropriate for equilibrium, with magnesiowüstite and spinel having Fe# of 0.166 and 0.11, respectively (that is, for peridotite mantle composition) (*8–11*). In contrast to spinel-magnesiowüstite relations, which are insensitive to the presence of other components, this result can only apply in the absence of Al_2O_3.

Fertile peridotites such as "pyrolite" (*12*) contain 3.0 to 4.0 weight % Al_2O_3, most of which should, in the lower mantle, reside in the Mg-rich perovskite phase, with lesser amounts in magnesiowüstite and Ca perovskite (*2*, *7*). In a peridotitic composition, the perovskite phase constitutes about 75% of

Table 1. Experimental data: pressure (*P*), temperature (*T*), and compositions. Experiments at 25 GPa in Mo capsules exhibited Fe loss to the capsule and precipitation of Mo-Fe alloy in the charge. Runs in Re capsules contained excess ReO_2 to maintain oxidizing conditions. MW, magnesiowüstite; OL, olivine; SP, spinel; OP, orthopyroxene; and PV, perovskite. Numbers in parentheses refer to Fe# and weight % Al_2O_3.

P (GPa)	*T* (°C)	Starting composition	Capsule	Final composition
20.4	1600	MW(0.28,0.5), OL(0.104,0.0)	Mo	MW(0.25,0.5), SP(0.16,0.4)
20.4	1600	MW(0.46,0.4), OL(0.104,0.0)	Mo	MW(0.36,0.3), SP(0.22,0.2)
25	1600	MW(0.17,5.0), OP(0.10,0.0)	Re	MW(0.125,0.1), PV(0.155,6.8)
25	1600	MW(0.17,5.0), OP(0.21,4.1)	Re	MW(0.168,0.1), PV(0.195,8.9)
25	1500	MW(0.17,5.0), OP(0.21,4.1)	Fe	MW(0.185,1.5), PV(0.185,4.3)*
25	1600	MW(0.46,0.4), OP(0.21,4.1)	Mo	MW(0.154,0.7), PV(0.180,4.0)
25	1600	MW(0.28,0.5), OP(0.10,3.6)	Mo	MW(0.094,0.3), PV(0.096,4.1)
25	1600	MW(0.17,5.0), OP(0.21,4.1)	Mo	MW(0.121,1.3), PV(0.169,4.5)*
25	1600	MW(0.17,5.0), OP(0.21,4.1)	Mo	MW(0.151,2.3), PV(0.188,5.0)

*A small amount of an unidentified aluminous phase was present.

B. J. Wood, Department of Geology, University of Bristol, Bristol BS8 1 RJ, UK.
D. C. Rubie, Bayerisches Geoinstitut, Universität Bayreuth, D-95440 Bayreuth, Germany.